J Mater Sci: Mater Electron (2022) 33:11002–11016

Microstructure and shear strength of Au-20wt%Sn solder joints fabricated by thermo-compression bonding for LED packages

Dong-hun Lee[1,2], Jae-il Jang[1], and Young-Ho Kim[1,*]

[1] Division of Materials Science and Engineering, Hanyang University, 04863 Seoul, Republic of Korea
[2] LED Business Team, Samsung Electronics, 17113 Yongin-si, Republic of Korea

Received: 1 December 2021
Accepted: 13 March 2022
Published online:
27 March 2022

ABSTRACT

Solder joints of Au-20wt%Sn (Au-20Sn) between real light-emitting diode Si chips and AlN substrates were fabricated using thermo-compression (TC) bonding. We investigated the microstructure of TC-bonded solder joints using scanning electron microscopy, transmission electron microscopy (TEM), and scanning transmission electron microscopy (STEM) and its effect on shear strength. The metallization system for the Au-20Sn solder consisted of Pt/Ti thin films on Si chips and an electroless Ni/Pd/Au layer on AlN substrates. The TC bonding was carried out at 280, 290, 300, and 310 °C for 0.2, 0.6, and 1.2 s. Samples were aged at 200 °C for up to 1000 h in a conventional oven. The performance of the solder joints was sensitive to joining temperature. When the solder joint was formed at a relatively low temperature, shear strength was low due to the unbonded regions in the solder joints. The shear strength increased with joining temperature and time. When the solder joints were formed at a relatively high temperature, shear strength was high. The solder joints were composed of δ-phase at both interfaces and ζ′-phase at the center. After aging at 200 °C for up to 1000 h, shear strength slightly decreased. The main fracture modes before and after aging were Si cohesive fracture and interfacial fracture between Si and Ti, respectively. TEM and STEM clearly indicated that the Pt layer remained at the solder interface after aging. The high shear strength was attributed to the strong interface between Pt and the Au-20Sn solder.

1 Introduction

As light-emitting diodes (LEDs) products are being diversified and their field of application is expanded to devices such as automobile lamps, drive current requirements that increase power consumption have increased. The heat produced by high-power LEDs must be dissipated through their substrates. Thus, a good thermally conductive interface between die and substrate is essential to maintain LED performance at

Address correspondence to E-mail: kimyh@hanyang.ac.kr

https://doi.org/10.1007/s10854-022-08079-y

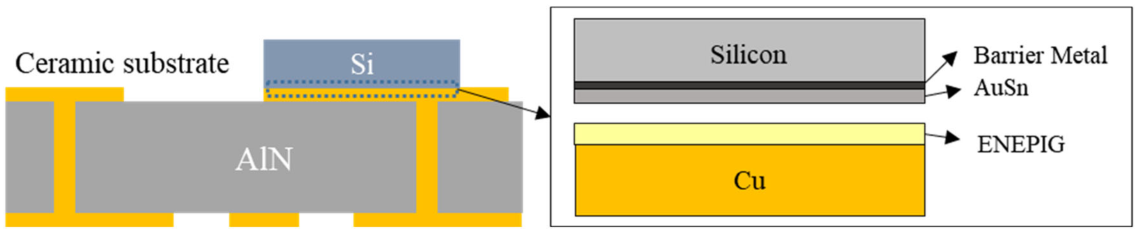

Fig. 1 Schematic of solder joints formed between Si LED Chip and AlN substrate

Table 1 Thermo-compression Bonding process conditions

Conditions	1	2	3	4	5	6	7	8	9	10	11	12
Joining Temp.	280 °C			290 °C			300 °C			310 °C		
Joining Time (s)	0.2	0.6	1.2	0.2	0.6	1.2	0.2	0.6	1.2	0.2	0.6	1.2

the maximum allowable junction temperature [1]. Among the die attachment materials used in high-power LED packages, such as Ag paste, Sn-based solders, and eutectic Au-Sn solder, Au-20wt%Sn (Au-20Sn) solder is notable due to its superlative thermal resistance [2]. In addition, the high thermal conductivity of Au–20Sn makes it particularly useful for bonding high-power devices that demand a good capacity for heat dissipation [3]. Au–20Sn solder also provides advantages such as flux-less soldering and beneficial mechanical and electrical properties [4, 5]. Use of flux is prohibited, particularly for LEDs, micro-electro-mechanical systems (MEMS), laser diodes, and biomedical instruments packaging, because the flux residue adversely affects the optical performance and can induce corrosion [6, 7].

A system of Pt/Ti metallization on semiconductors has been widely used for Au-Sn soldering [8–13]. A Ti layer provides adhesion between Si and Pt [7]. This Pt/Ti system has a good thermal stability [9], and Pt is not easily oxidized and has a low dissolution rate with Sn. With these two beneficial characteristics, a Pt layer can play the roles of both an oxidation protection layer and a diffusion barrier layer [10]. Ni and Cu are generally used as surface finish metals [14–19]. Ni and Cu are the two most common metals in direct contact with solder and are widely used as a surface finish layer on metal bond pads in the electronic packaging industry. In particular, electroless Ni/Au metallization has become popular since it reduces processing costs while providing a good interfacial diffusion barrier [16]. Reflow soldering using Au-Sn solders is the most widely used method for attaching LED chips to substrates [1, 3, 11, 16]. Recently, thermo-compression (TC) bonding has been investigated for Au-Sn soldering [20]. When considerable pressure is applied during soldering, good contacts are established and sufficient heat is transferred to the solder and metallization layer [21]. After contact between the Au-20Sn solder and the metallization layer, the solder is heated above its melting temperature so that it wets the metallization layer. However, a thin Pt layer might be dissolved completely into the molten solder during soldering. If such dissolution occurs, the poor wettability of the solder on the exposed Ti layer leads to de-bonding at the interface [11, 22]. Intermetallic compounds (IMCs) such as PtSn and $PtSn_4$ [8, 13] are known to form at the interface between Pt and Au-20Sn solder. As a result, a non-uniform joint is formed, and excessive growth of the IMC layer can degrade the performance of the solder joints [13]. Microstructure characterization of the interface between Pt and Au-20Sn solder is important for understanding how to optimize soldering conditions to obtain high-quality solder joints.

Joining temperature and time are the main factors that affect the quality and reliability of solder joints. Han et al. proposed the optimum process conditions for Au-Sn TC bonding based on of shear force measurements [20]. However, the effect of the microstructure in solder joints was not investigated.

In the present study, different microstructures of solder joints were developed based on joining conditions. We fabricated Au-20Sn solder joints using TC bonding with real LED chips and AlN substrates. The

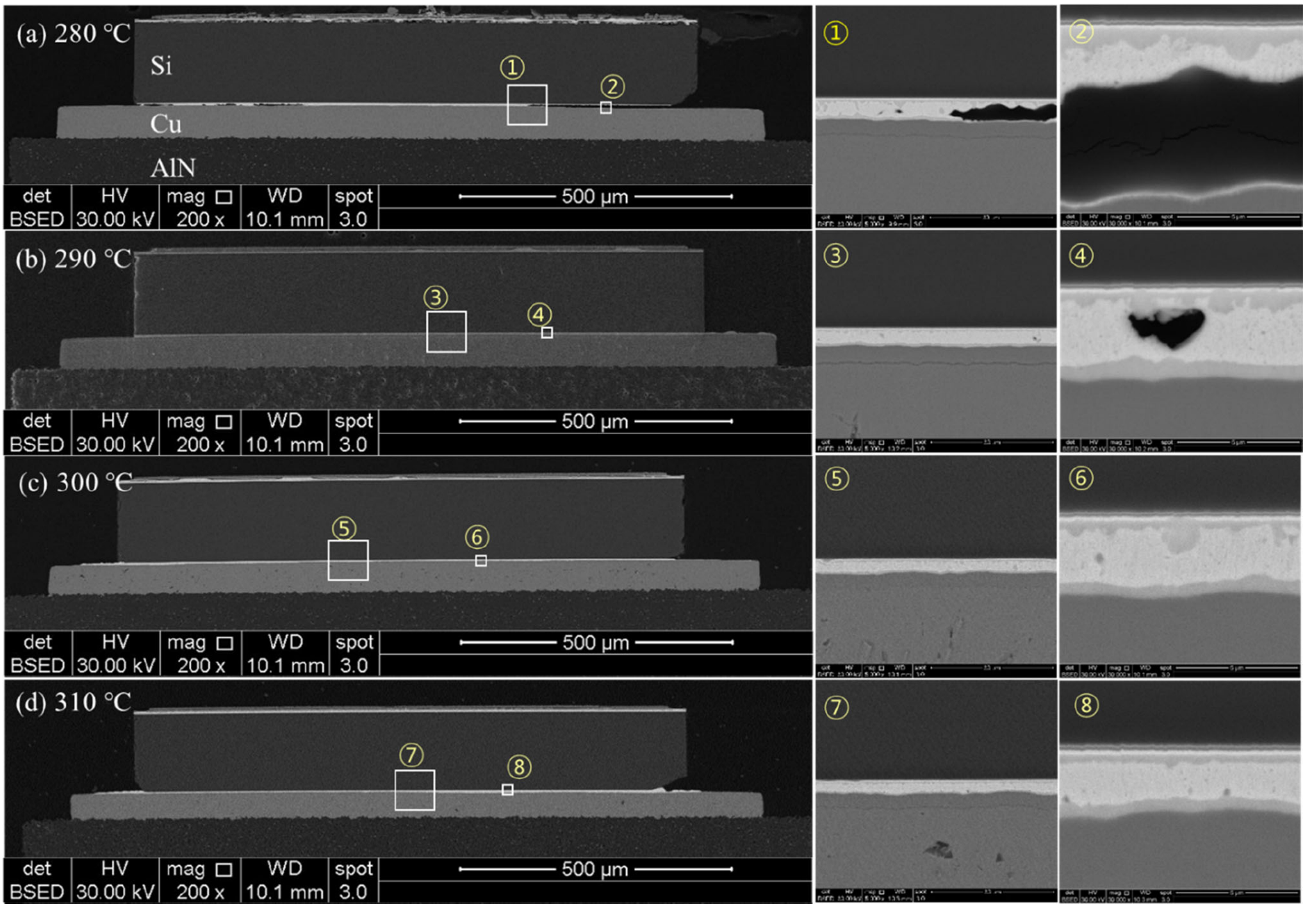

Fig. 2 The SEM images of cross-sectional solder joints formed **a** 280 °C, **b** 290 °C, **c** 300 °C, and **d** 310 °C. Joining time was 0.2 s for all samples

metallization system for the Au-20Sn solders consisted of Pt/Ti thin films on LED chips and a Ni/Cu finish on AlN substrates. We characterized the microstructures of the solder joints and investigated their effects on joint quality and long-term reliability.

2 Experimental

The LED package structure used in this study is shown in Fig. 1 and is composed of a 3 W blue LED Si chip and an AlN substrate. The back side of the Si chip was metallized with Pt/Ti barrier layers. This films of Ti (0.15 μm), Pt (0.05 μm), Ti (0.15 μm), and Pt (0.2 μm) were sputtered sequentially on the Si chip using direct current magnetron sputtering. The tolerance of thin film thickness was ± 5%. Then, Au-20wt%Sn solder was co-deposited using an e-beam evaporator. The AlN ceramic substrate was electroplated with Cu using the direct plating method [23]. The surface finish, electroless Ni/Pd/Au (ENEPIG), was deposited on the Cu layer. The thicknesses of the Ni(P), Pd, and Au layers were 5.0, 0.1, and 0.15 μm, respectively. The joining process for die attachment was carried out via thermo-compression (TC) bonding at 280, 290, 300, and 310 °C with a bond force of 1.47 N for 0.2, 0.6, and 1.2 s in N_2. Table 1 lists the applied TC bonding conditions. After TC bonding, an aging test was carried out at 200 °C for 250, 500, and 1000 h in a conventional oven to evaluate the long-term reliability of the solder joints.

Cross-sections of the Au-20Sn solder joints were characterized using scanning electron microscopy (SEM/ Inspection F, FEI, USA), transmission electron microscopy (TEM/ NEO ARM, JEOL, Japan) with energy dispersive X-ray spectroscopy (EDS), and scanning transmission electron microscopy (STEM). Samples for (S)TEM analyses were prepared using an

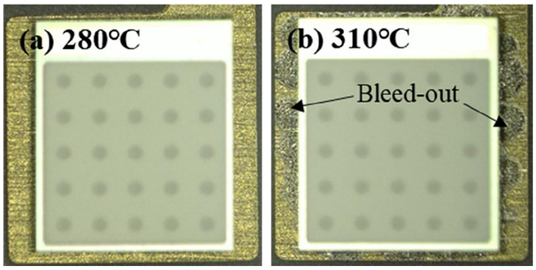

Fig. 3 Comparison of bleed-out images, as-joined samples **a** 280 °C, 0.2 s, **b** 310 °C, 0.2 s

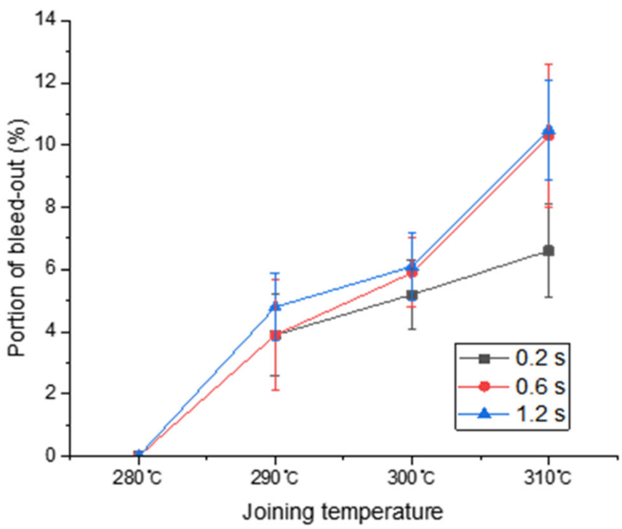

Fig. 4 The portion of bleed-out region in as-joined solder joints

focused ion beam (FIB/ SCIOS, FEI, USA) system, and analyses were performed using NEO ARM equipment. Samples for SEM analysis were prepared using standard metallographic methods. The die shear test was carried out using a high-speed ball shear tester (Dage 4000, Nordson, UK) to evaluate solder joint strength. The shear height was 50 µm across the substrate, and the shear speed was 500 µm/s. The shear strength was defined as the maximum load at fracture divided by the total joint area of the chip. At least 10 samples were tested under each condition to calculate the average shear strength. The fracture modes were analyzed with optical microscopy (OM) and SEM (FEI, Inspection F).

3 Results and discussion

3.1 Microstructural characterization of Au-20Sn solder joints

Figure 2 shows typical cross-sectional SEM images of the Au-20wt%Sn solder joints in the LED packages. The images reveal an unbonded region was found in the solder joints formed at 280 °C, and there were voids in the Au-Sn solder joints formed at 290 °C. In contrast, good solder joints were formed with no large voids at 300 °C and 310 °C. The proportion of unbonded region in the solder joint depended on joining temperature. The bonded region increased in size with increasing joining temperature. There were no unbonded regions found in the solder joints formed at 300 °C or 310 °C. In addition, as the temperature increased, the flowability of the Au-Sn solder increased, causing Au-Sn solder to extrude around the chip, known as bleed-out. Figure 3 shows top views of two chips joined with AlN substrates: one without bleed-out (Fig. 3a) and one exhibiting solder bleed-out from the edge of the chip (Fig. 3b, bleed-out marked with arrows). Figure 4 shows the effects of joining temperature and time on the proportion of bleed-out, calculated as a ratio of the bleed-out area around the chip to the total chip area. The proportion of bleed-out increases with increased joining temperature and time. In a multi-chip package or a package with a small gap between electrodes, the increased bleed-out region induces a risk of short failure. Therefore, considering the proportions of unbonded regions and the bleed-out regions, the optimal joining temperature is 300 °C.

Enlarged cross-sectional SEM micrographs of solder joints in the as-joined samples are presented in Fig. 5. As the joining temperature increased, solder joint thickness decreased due to the bleed-out effect. The solder joints were composed of layers of δ-phase (dark constituent) at the Pt and Ni interfaces and of ζ′-phase (bright constituent) at the center of the solder joint in all samples. Our observation was consistent with previous results of thin Au-Sn solder joints [24, 25]. Since the Sn-rich δ-phase has a lower surface tension than the Au-rich ζ′-phase [26], the Sn-rich δ-phase tends to migrate toward the edge of the solder joint, leaving the center as Au-rich ζ′-phase [24]. In addition, Pt layers (thin white layers marked with arrows in Fig. 5) were observed in all samples.

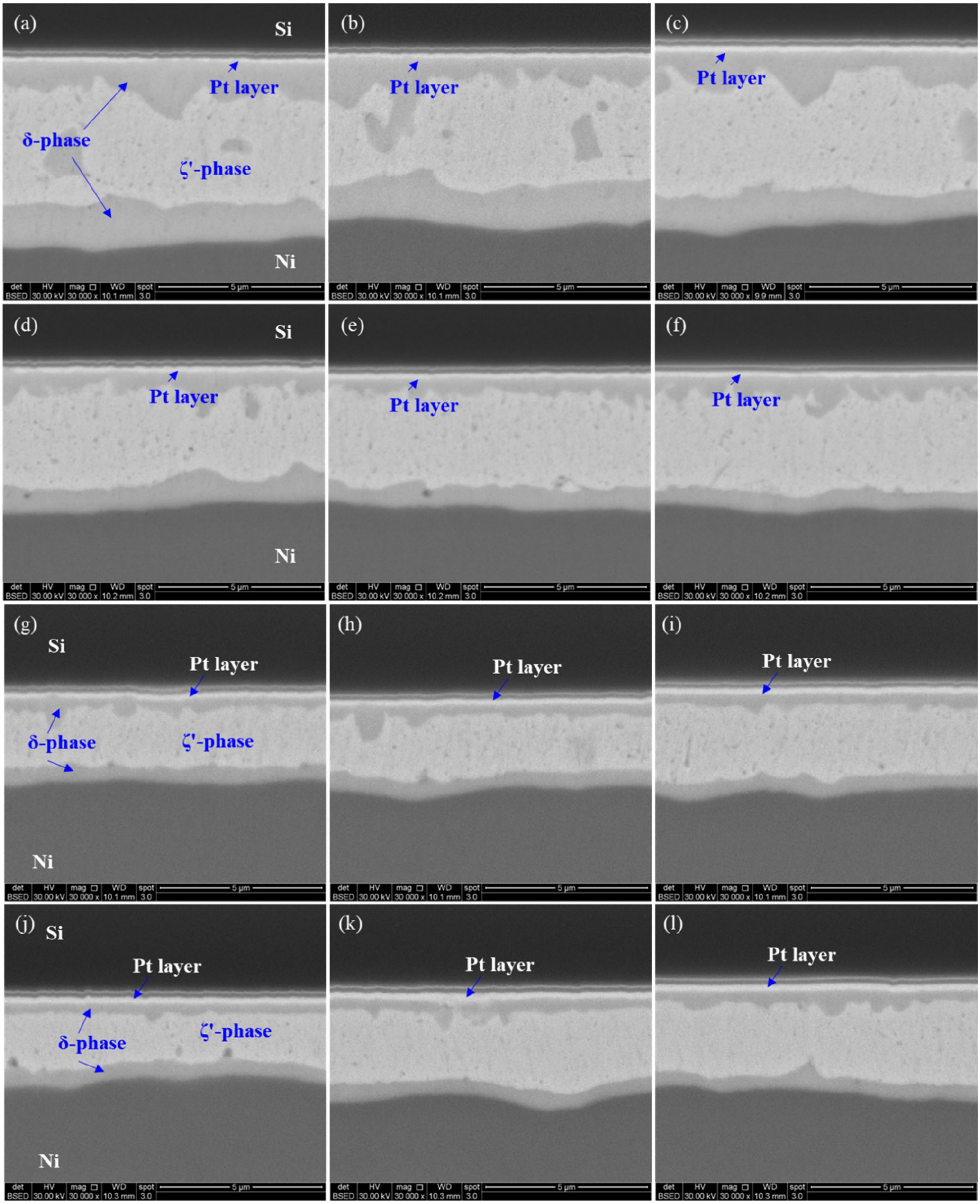

Fig. 5 Cross-sectional SEM images of the solder joints formed; **a** 280 °C, 0.2 s, **b** 280 °C, 0.6 s, and **c** 280 °C, 1.2 s,**d** 290 °C, 0.2 s, **e** 290 °C, 0.6 s, and **f** 290 °C, 1.2 s, **g** 300 °C, 0.2 s, **h** 300 °C, 0.6 s, and **i** 300 °C, 1.2 s, **j** 310 °C, 0.2 s, **k** 310 °C, 0.6 s, and **l** 310 °C, 1.2 s

Two representative samples of solder joints were prepared using FIB to analyze the solder joints more clearly under TEM: a solder joint formed at 300 °C for 0.2 s and one formed at 310 °C for 1.2 s. In order to characterize the phases more clearly, solder joints were observed in STEM mode in addition to TEM mode. Figures 6 and 7 show the cross-sectional (S)TEM images of the solder joints formed at 300 °C for 0.2 s and at 310°C for 1.2 s, respectively. Chemical analyses of the regions marked with numbers in Figs. 6 and 7 were preformed using EDS and are summarized in Tables 2 and 3. Figures 6a and 7a are low magnification STEM images of whole Au-20Sn solder joints between the Pt/Ti and Ni interfaces. The microstructures observed in these STEM images are similar to those in the SEM images shown in Fig. 5g and l. Magnified (S)TEM images near the Pt interfaces are shown in Figs. 6b, c and 7b, c and near the Ni interfaces in Figs. 6d, e, and 7d, e. The Pt/Ti double layers, Ni(P) layer, δ-phase, and ζ′-phase were easily identified using EDS line scan and point analyses (Tables 2 and 3). The thicknesses of Pt/Ti double layers in Figs. 6 and 7 are almost the same as the set values explained in the Experimental section except where the Pt layers were in contact with the Au-20Sn solders, as these Pt layers are consumed during the reaction with Au-20Sn solder during TC bonding. The reduction in Pt thickness was minimal in both samples. This thickness reduction is reasonable since the dissolution rate of Pt into the Au-20Sn solder was approximately 0.6 μm/min at 330 °C [11]. A considerable amount of Pt was detected in the δ-phase near the Pt interface since Pt atoms dissolved into the δ-phase layer. The Sn concentration was constant

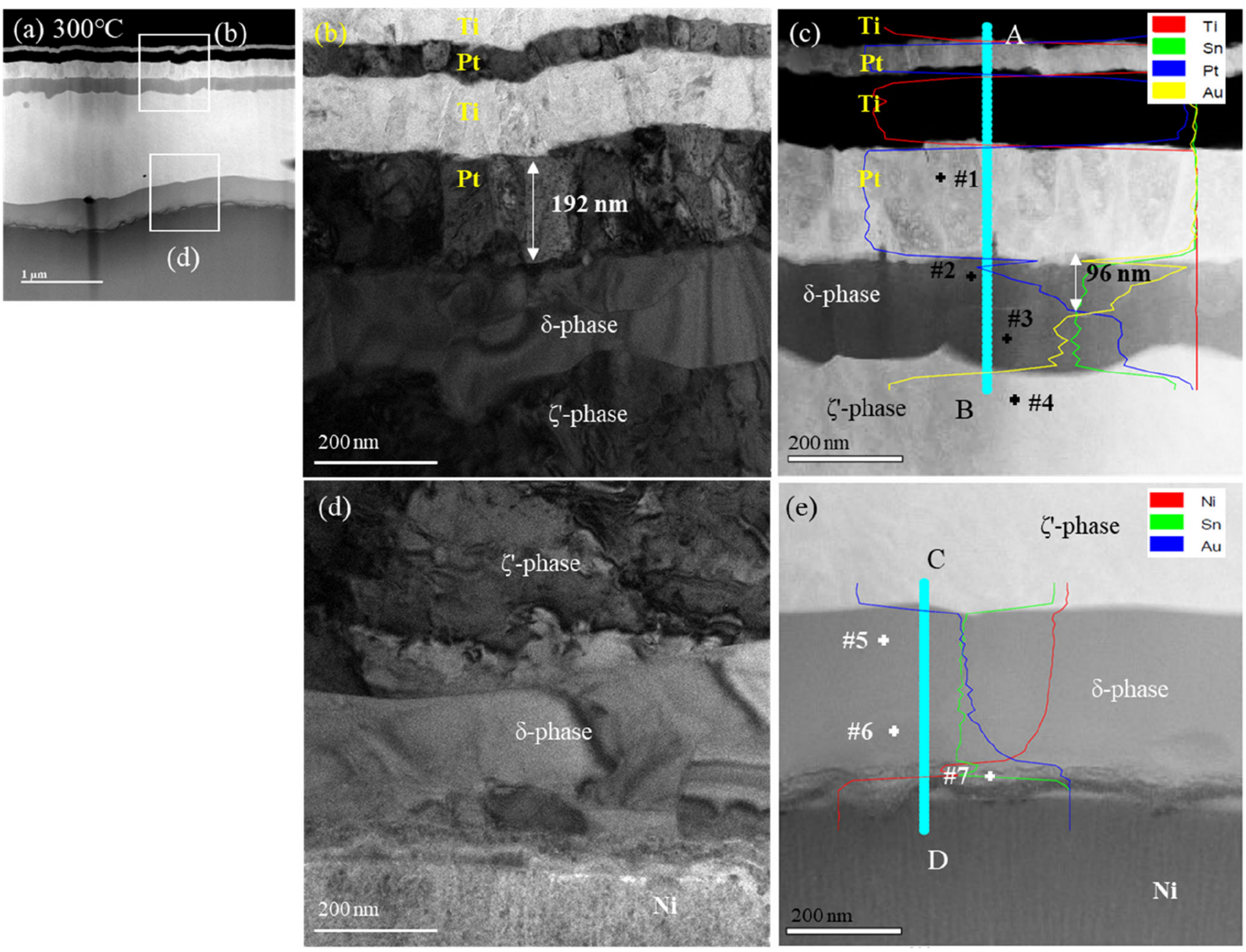

Fig. 6 Cross-sectional (S)TEM images of the solder joint formed at 300 °C, 0.2 s; **a** a low magnification STEM image; **b** a magnified TEM image of region **b** in **a** near Pt interface; **c** STEM image and EDS line scan from A and B; **d** a magnified TEM image of region **d** in **(a)** near Ni interface; **e** STEM image and EDS line scan from C and D

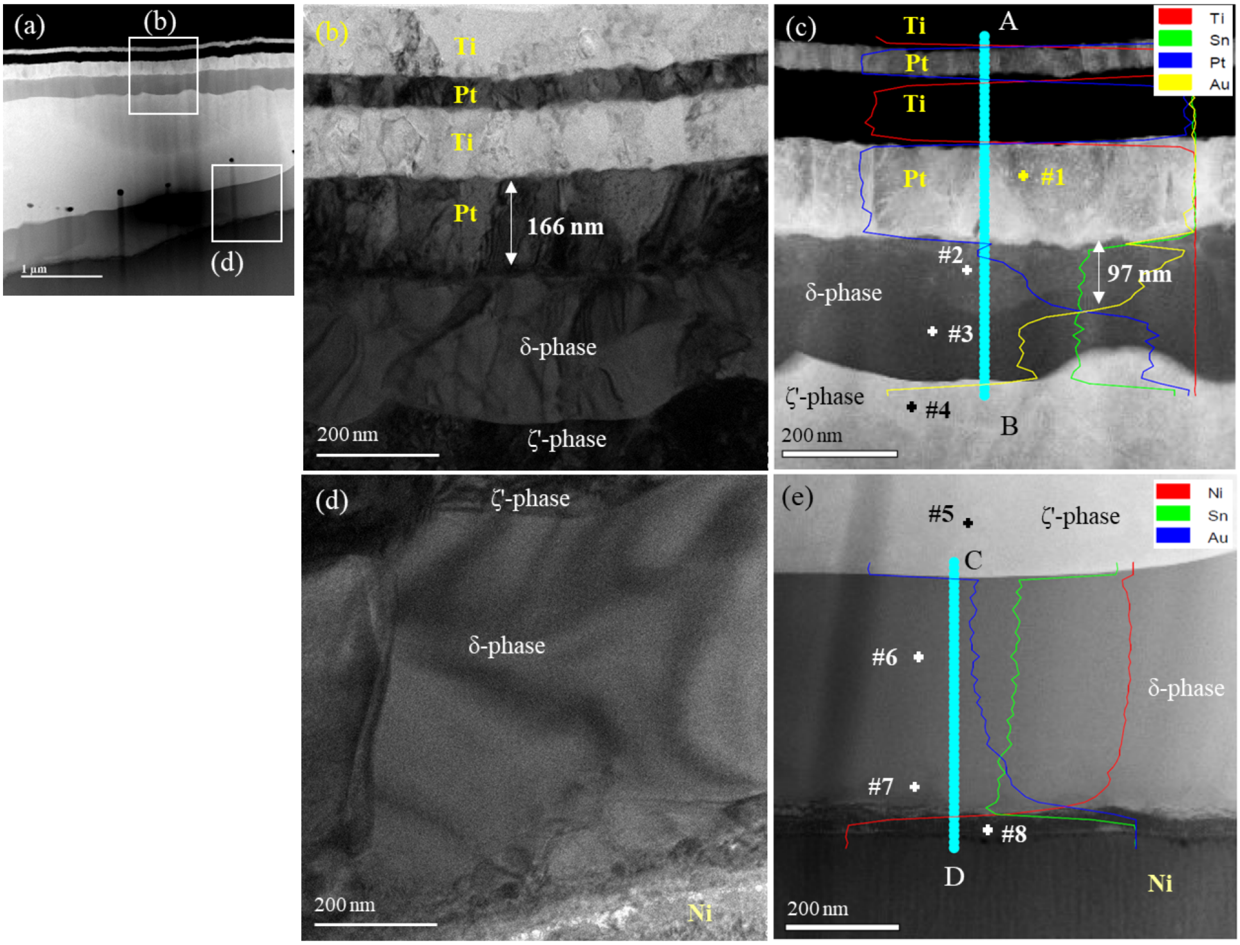

Fig. 7 Cross-sectional (S)TEM images of the solder joint formed at 310 °C, 1.2 s; **a** a low magnification STEM image; **b** a magnified TEM image of region **b** in **a** near Pt interface; **c** STEM image and EDS line scan from A and B; **d** a magnified TEM image of region **d** in **a** near Ni interface; **e** STEM image and EDS line scan from C and D

Table 2 EDS results of corresponding positions shown in Fig. 9

Analysis Point	Composition (at%)						Phase
	Ti	Pt	Sn	Au	Ni	P	
(c) #1		100					Pt
#2		44.69	43.63	11.68			(Pt, Au)Sn
#3		16.31	48.56	35.13			(Au, Pt)Sn
#4			10.91	89.09			ζ'-Au_5Sn
(e) #5			48.47	41.49	10.04		(Au, Ni)Sn
#6			48.65	24.22	27.13		(Au, Ni)Sn
#7					82.59	17.41	Ni-P

throughout this δ-layer, which can be divided into two sublayers: a Pt-rich (Pt,Au)Sn layer near the Pt interface and an Au-rich (Au,Pt)Sn layer far from the Pt interface. Formation of PtSn phase has been reported between an Au-Sn layer and Pt [9, 12]. Pt reacts preferentially with Sn in Au-Sn solder to produce an intermediate layer [9]. Detailed analysis of these two layers is in progress. No other compounds, such as $PtSn_4$, were observed. In addition, Ni was detected in the δ-phase near the Ni(P) interfaces. Ni atoms from the Ni(P) layer dissolved into the δ-phase layer to form (Au,Ni)Sn phase, as δ-phase has

Table 3 EDS results of corresponding positions shown in Fig. 10

Analysis Point	Composition (at%)						Phase
	Ti	Pt	Sn	Au	Ni	P	
(c) #1		100					Pt
#2		41.98	45.37	12.65			(Pt, Au)Sn
#3		12.35	47.91	39.74			(Au, Pt)Sn
#4			10.51	89.49			ζ'-Au_5Sn
(e) #5			11.36	88.64			ζ'-Au_5Sn
#6			51.31	41.88	6.80		(Au, Ni)Sn
#7			48.85	25.45	25.71		(Au, Ni)Sn
#8					78.30	21.70	Ni-P

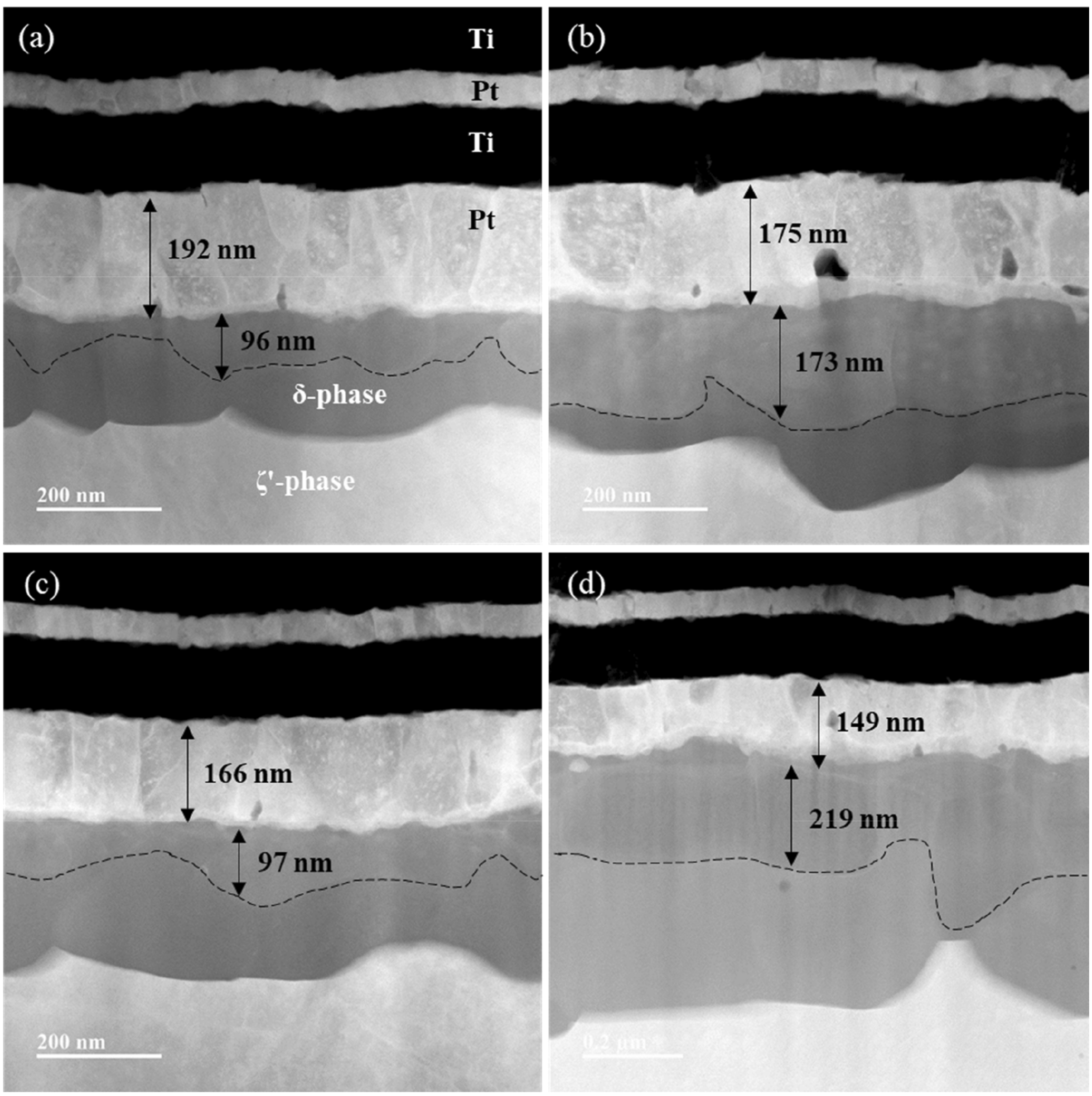

Fig. 8 Cross-sectional STEM images of the solder joints; **a** 300 °C, 0.2 s, as-joined; **b** 300 °C, 0.2 s, aged for 1000 h; **c** 310 °C, 1.2 s, as-joined; **d** 310 °C, 1.2 s, aged for 1000 h

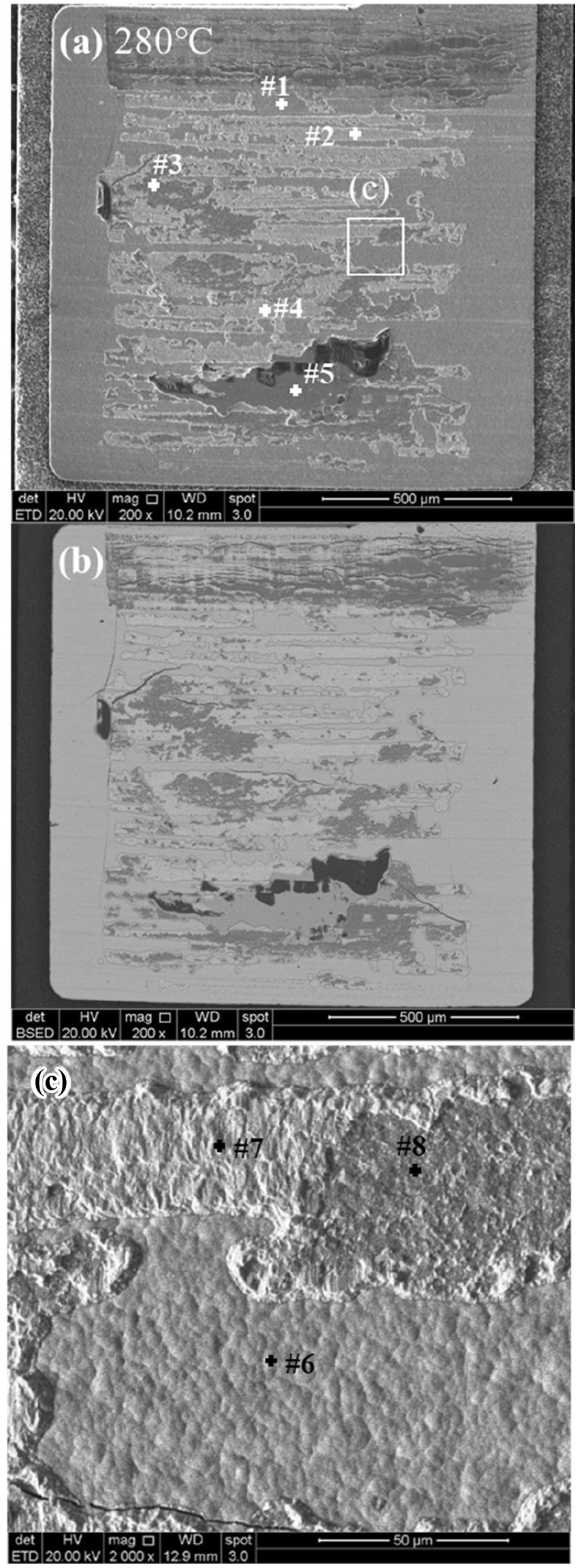

Fig. 10 Typical SEM fractographies of the solder joint (AlN substrate side) which was formed at 280 °C, 0.2 s, **a** SE mode, **b** BSE mode, and **c** a magnified SE image shown (**c**) in (**a**)

high Ni solubility [16]. In previous studies, $(Ni,Au)_3Sn_2$ phase has been found at the Ni interface [15–17, 24, 25]. This phase was not identified in our experiment, possibly because it could not form in very short soldering times (1.2 s or less) or because the $(Ni,Au)_3Sn_2$ layer was too thin to be detected.

Figure 8 shows STEM images of the sample joined at 300 °C for 0.2 s and at 310 °C for 1.2 s before (as-joined samples) and after aging for 1000 h. Since the interfaces between Pt and Au-20Sn solder are important, these regions were closely observed. The same STEM images of as-joined samples (Figs. 6c and 7c) are presented again in Fig. 8a and c for comparison with images of the aged sample. The decrease in thickness of the Pt layer was greater with higher joining temperatures and longer joining times, as the Pt atoms react and dissolve into the molten solder during TC bonding. After aging, the thickness of the Pt layer was further reduced due to solid-state reaction with Au-20Sn solder. However, a considerable portion of the Pt layer remained. The Pt-rich (Pt,Au)Sn layer and the Au-rich (Au,Pt)Sn layer could be distinguished due to the contrast difference within the δ-phase. The interface between these two

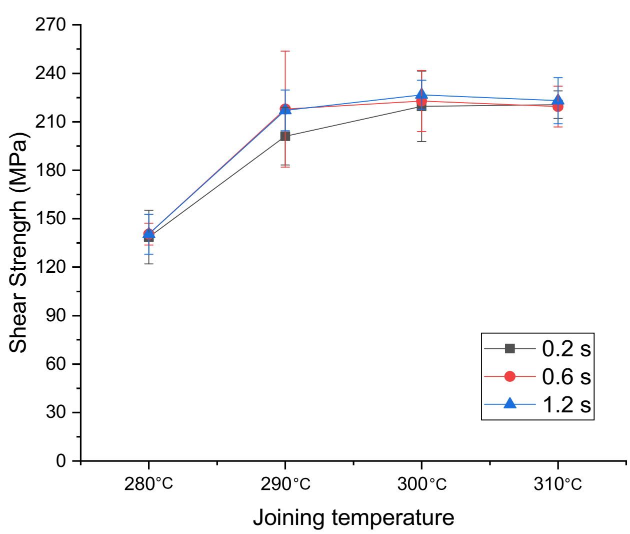

Fig. 9 Shear strength of the as-joined solder joints as functions of joining temperature and time

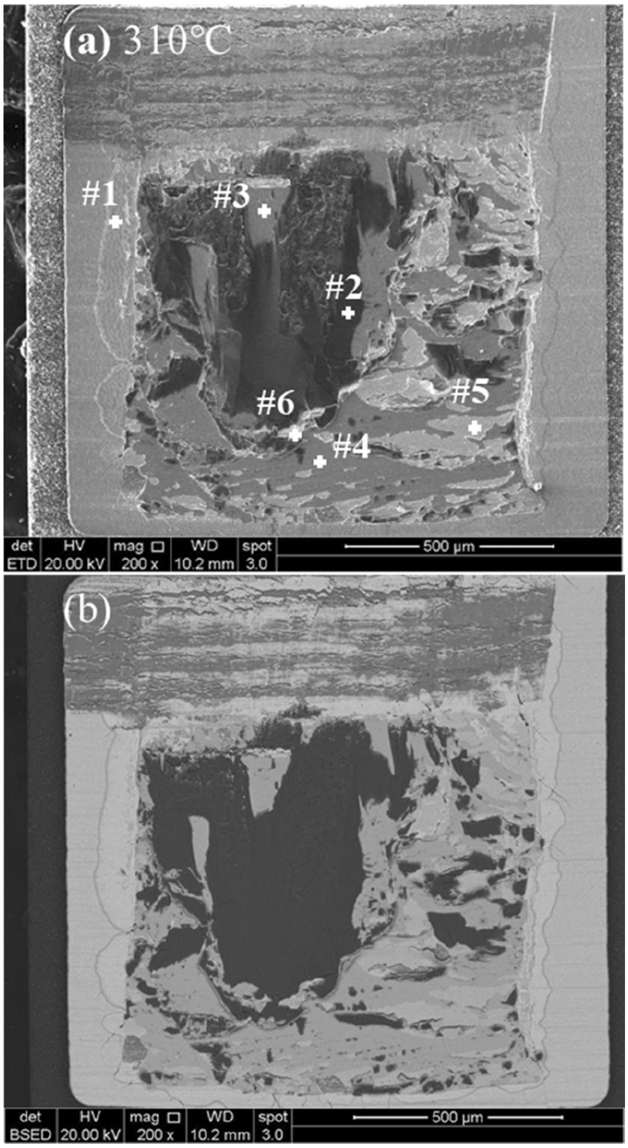

Fig. 11 Typical SEM fractographies of the solder joint (AlN substrate side) which was formed at 310 °C, 0.2 s, **a** SE mode, **b** BSE mode

layers is indicated with a dotted line for clarity. The average thickness of the Pt-rich (Pt,Au)Sn layers was 96 nm in the sample joined at 300 °C for 0.2 s and 97 nm in the sample joined at 310 °C for 1.2 s. The thickness of the Pt-rich (Pt,Au)Sn layer increased with time since Pt atoms continuously diffused into the solder during aging. After 1000 h, the Pt-rich (Pt,Au)Sn layer and the total δ-phase layer became quite thick.

3.2 Shear strength and fracture analysis

The effects of joining temperature and time on the shear strength of the as-joined Au-20Sn solder joint are shown in Fig. 9. The shear strength of the solder joints formed at 280 °C was about 140 MPa and increased with increasing joining temperature and time. Joining temperature was the more sensitive factor in its influence on shear strength. The shear strength of the solder joints formed at 280 °C was relatively low since solder joints only partially formed, as seen in Fig. 2. All shear strength values were measured to be about 200 MPa when the solder joints were formed at 290 °C, 300 °C, and 310 °C. In previous studies with similar metallization systems, the shear strength of Au-20Sn solder joints was between 24.5 MPa and 152 MPa [24, 25, 27]. Even considering that the shear strength can be affected by joining conditions and specimen geometries, the values obtained in our study were much higher than those of previous studies. High strength values mean that the Au-Sn solder joints are very strong.

After the shear test, the fracture modes were characterized. Observation of fracture surfaces revealed several fracture modes (substrate side) (Figs. 10 and 11). The chemical compositions of the regions marked with numbers in Figs. 10 and 11 were analyzed using EDS and are summarized in Tables 4 and 5. Figure 10 shows SEM images of the fracture surfaces of the solder joints (AlN substrate side) formed at 280°C for 0.2 s. Chemical compositional analyses of regions #1 in Fig. 10a and #6 in Fig. 10c indicate that these regions were ENEPIG layers. The magnified SE image of region #6 clearly showed the morphology of an as-plated surface. These regions were identified as unbonded regions. Figure 11 displays SEM images showing the fractured surface of the solder joints (AlN substrate side) formed at 310°C for 0.2 s. Region #2 is composed of Au and Sn (Table 5). This region corresponds to the solder bleed-out region, as seen in Fig. 3b. The composition of region #4 is 100% Si, indicating that fracture occurred inside the Si chip. The BSE image in Fig. 11 shows that the Si cohesive fracture was the main fracture mode in this sample, as has been reported in previous studies [25]. Considering SEM fractographies and EDS analyses, the fracture modes can be classified into Si cohesive fracture, interfacial fracture between Si and Ti adhesion layer, solder fracture, and unbonded region fracture. The fractured surfaces of

Table 4 EDS results of corresponding positions shown in Fig. 13

Analysis point		Composition (at%)							Phase
		Ti	Pt	Sn	Au	Pd	Ni	P	
(a)	#1				40.29	13.41	46.3		ENEPIG
	#2			11.37	88.63				Au-Sn Solder
	#3			4.05			82.99	12.96	Solder/ Ni(P)
	#4			14.52	75.37		10.11		Au-Sn Solder
	#5	63.69	26.85	9.46					Ti/Pt Layer
(b)	#6				42.08	13.07	44.85		ENEPIG
	#7			12.49	87.51				Au-Sn Solder
	#8						87.05	12.95	Ni(P)

Table 5 EDS results of corresponding positions shown in Fig. 14

Analysis Point		Composition (at%)							Phase
		Si	Ti	Pt	Sn	Au	Ni	Cu	
(a)	#1				13.97	86.03			Au-Sn solder
	#2	100							Chip - Si
	#3		57.47	42.53					Ti/Pt Layer
	#4		66.23	33.77					Ti/Pt Layer
	#5				63.11	36.89			Au-Sn solder
	#6				65.55	34.45			Au-Sn solder

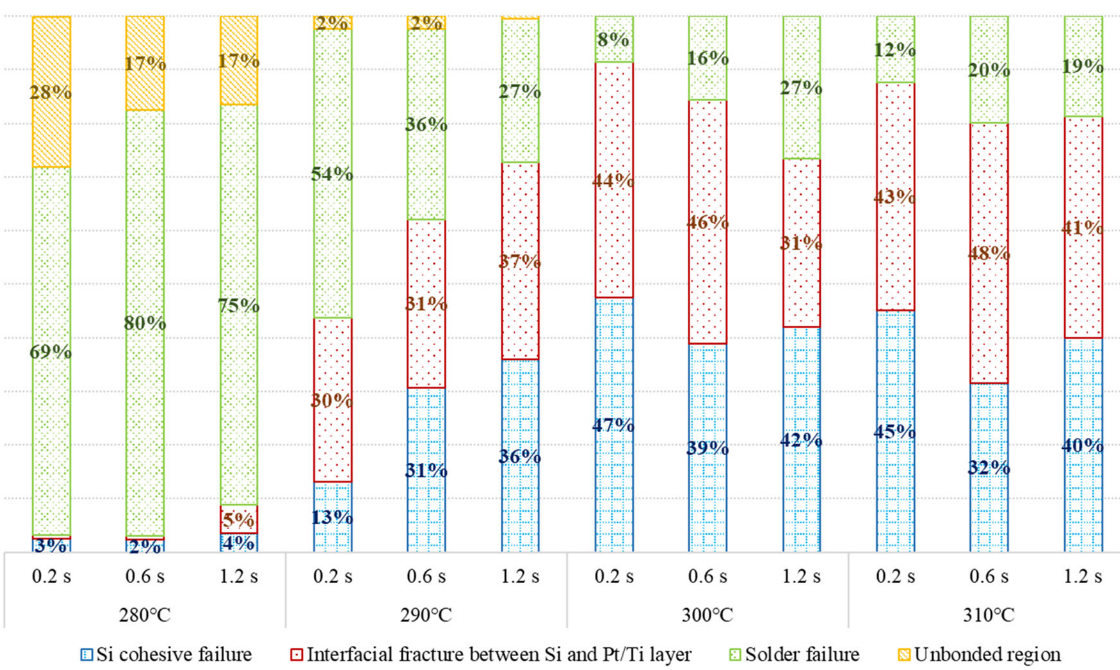

Fig. 12 Fracture mode distribution of the as-joined solder joints after shear test

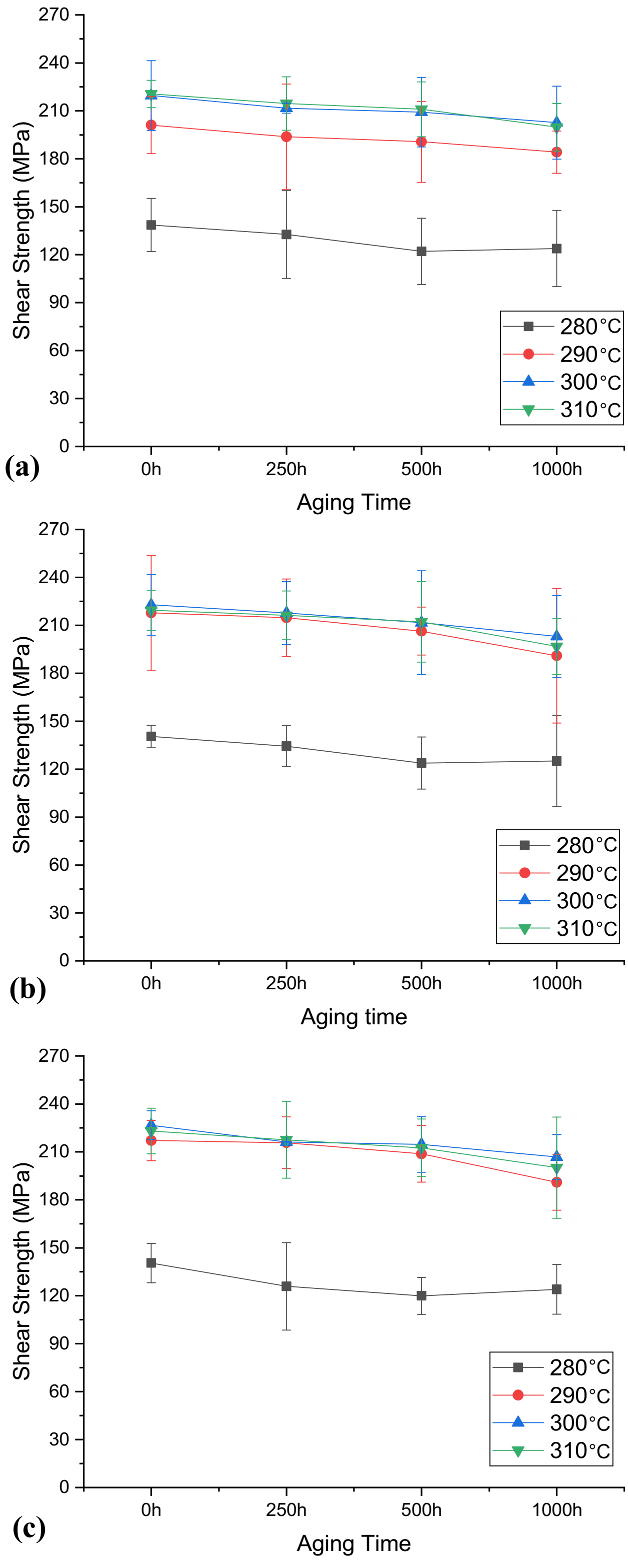

Fig. 13 Variation of shear strength with aging time. Solder joints were formed at various temperatures for **a** 0.2 s, **b** 0.6 s, and **c** 1.2 s

Fig. 14 Fracture mode distribution with aging time. The solder joints were formed at 280 °C, 290 °C, 300 °C, and 310 °C for **a** 0.2 s, **b** 0.6 s, and **c** 1.2 s

all samples were characterized after performing the shear test, and the distribution of fracture modes of the as-joined samples is presented in Fig. 12. The proportion of unbonded region was 17–28% in the samples joined at 280°C, while unbound regions were not observed in the samples joined at 300 °C and 310 °C. A relatively large proportion of unbonded region in the solder joints indicates that the solder joint is very weak; the shear strengths of these joints were low. Unbonded regions and voids in the solder joints also degrade their thermal performance [2]. As joining temperature increased, the ratio of Si cohesive fracture to interfacial fracture between Si and Ti layer increased. These two fracture modes indicate that the Au-20Sn solder strength is higher than the Si cohesive strength and the interfacial strength between Si and Ti. The shear strength of Au-20Sn solder has been measured to be about 275 MP [28], which is much higher than the shear strength of the Au-20Sn solder joints obtained in this study. When the thin Pt layer is completely dissolved into the molten solder, de-bonding due to spalling can occur door to poor wettability of the solder over Ti [11, 21]. However, a considerable amount of the Pt layer remained during soldering, as shown in Figs. 6 and 7. The interface between Au-20Sn solder and the Pt layer should be strong [27], as reflected by the very high shear strengths observed from these samples (Fig. 9).

Figure 13 shows the changes to shear strength in response to aging at 200°C. As the aging time increased to 1000 h, the shear strength slightly decreased in all samples. The trend of the shear strength decrease with increased aging time was independent of joining temperature and joining time. The shear strength was above 200 MPa after aging at 200 °C for 1000 h in the samples joined at 300 °C or 310 °C. The distribution of fracture modes of the aged samples is presented in Fig. 14. There was no remarkable change to the fracture mode distribution upon aging in any of the samples. A considerably large proportion of unbonded regions was found in the sample joined at 280 °C, even after aging. The main fracture modes were Si cohesive fracture and interfacial fracture between Si and Ti in the aged samples joined at 300 °C and 310 °C. The thickness of the Pt layer in contact with Au-20Sn solder was

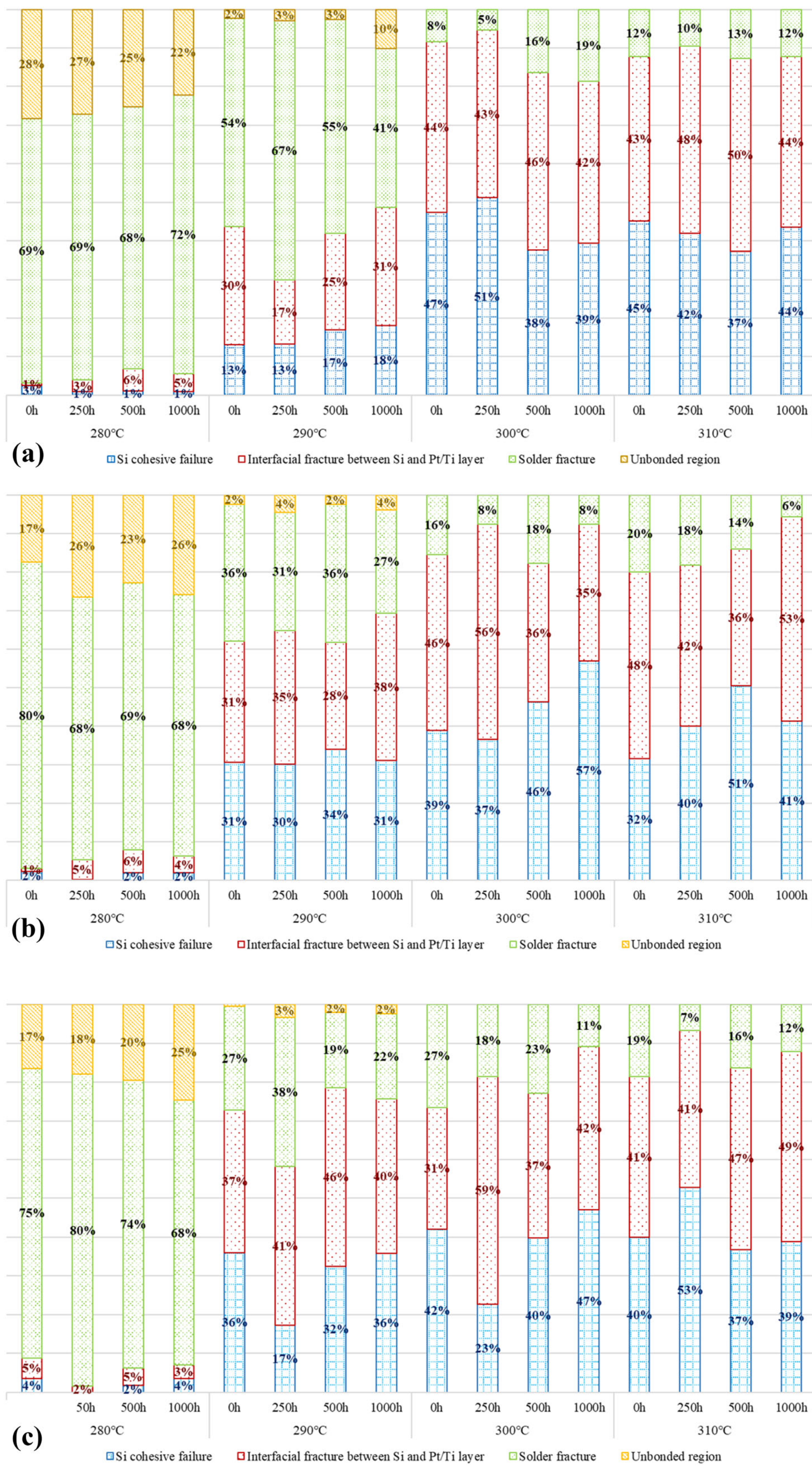
(a)
28% 69% 1% 3%
27% 69% 3% 1%
25% 68% 6% 1%
22% 72% 5% 1%
2% 54% 30% 13%
3% 67% 17% 13%
3% 55% 25% 17%
10% 41% 31% 18%
8% 44% 47%
5% 43% 51%
16% 46% 38%
19% 42% 39%
12% 43% 45%
10% 48% 42%
13% 50% 37%
12% 44% 44%
0h 250h 500h 1000h 0h 250h 500h 1000h 0h 250h 500h 1000h 0h 250h 500h 1000h
280°C 290°C 300°C 310°C
Si cohesive failure
Interfacial fracture between Si and Pt/Ti layer
Solder fracture
Unbonded region
(b)
17% 80% 1% 2%
26% 68% 5%
23% 69% 6% 2%
26% 68% 4% 2%
2% 36% 31% 31%
4% 31% 35% 30%
2% 36% 28% 34%
4% 27% 38% 31%
16% 46% 39%
8% 56% 37%
18% 36% 46%
8% 35% 57%
20% 48% 32%
18% 42% 40%
14% 36% 51%
6% 53% 41%
0h 250h 500h 1000h 0h 250h 500h 1000h 0h 250h 500h 1000h 0h 250h 500h 1000h
280°C 290°C 300°C 310°C
Si cohesive failure
Interfacial fracture between Si and Pt/Ti layer
Solder fracture
Unbonded region
(c)
17% 75% 5% 4%
18% 80% 2%
20% 74% 5% 2%
25% 68% 3% 4%
27% 37% 36%
3% 38% 41% 17%
2% 19% 46% 32%
2% 22% 40% 36%
27% 31% 42%
18% 59% 23%
23% 37% 40%
11% 42% 47%
19% 41% 40%
7% 41% 53%
16% 47% 37%
12% 49% 39%
50h 500h 1000h 0h 250h 500h 1000h 0h 250h 500h 1000h 0h 250h 500h 1000h
280°C 290°C 300°C 310°C
Si cohesive failure
Interfacial fracture between Si and Pt/Ti layer
Solder fracture
Unbonded region

reduced by aging. However, a fairly thick Pt layer remained, as seen in Fig. 8. High shear strengths above 200 MPa observed after aging suggest that the solder joints have high long-term reliability.

4 Summary

Au-20wt%Sn solder joints were fabricated between LED Si chips and AlN substrates by TC bonding.

1. The microstructure of the solder joints was characterized using SEM and (S)TEM with EDS. The solder joints were composed of δ-Au-Sn phase at both interfaces and ζ′- Au_5Sn phase at the center. The δ-layer at the Pt interface was divided into a Pt-rich (Pt,Au)Sn layer and an Au-rich (Au,Pt)Sn layer. After aging, the thickness of the Pt-rich (Pt,Au)Sn layer increased. A fairly thick Pt layer remained even though Pt reacts with Au-20Sn solder during TC bonding and aging.
2. When TC bonding was carried out at 280 °C, the shear strength of the solder joints was relatively low since the solder joints formed only partially. The shear strength increased with increasing joining temperature and time.
   When TC bonding was carried out at 300 and 310 °C, unbonded regions were not observed and the shear strength of the solder joints was very high. Since the interface between Pt and Au-20Sn solder is strong, Si cohesive fracture and interfacial fracture between Si and the Ti adhesion layer occurred. When the joining temperature was high, the proportion of solder bleed-out increased due to the increased flowability of the Au-Sn solder. Increased bleed-out induces a risk of short failure between the LED chips.
3. After aging at 200 °C for 1000 h, the shear strength slightly decreased, but the fracture mode did not change. Spalling was not observed in the Pt/Au-Sn solder interfaces since a fairly thick Pt layer remained after aging. As a result, the Au-20Sn solder joints maintained high shear strength even after aging, which means that they have a good long-term reliability.

Acknowledgements

This research was supported by an LED business team collaborative project between Hanyang University and Samsung Electronics Co. Ltd.

Author contribution

DL, JJ, and YK wrote the paper.

Data Availability

All data generated or analyzed during this study are included in this published article and its supplementary information files.

Declarations

Conflict of interest The authors declare no conflict of interest.

References

1. H.H. Kim, S.H. Choi, S.H. Shin, Y.K. Lee, S.M. Choi, S. Yi, Microelectron. Reliab. **48**, 445 (2008)
2. K. Chu, C. Lee, S.H. Park, Y. Sohn, J. Mater. Sci. Mater. Electron. **28**, 5174 (2017)
3. J.W. Yoon, H.S. Chun, S.B. Jung, Mater. Sci. Eng. A **473**, 119 (2008)
4. V. Grolier, R. Schmid-Fetzer, J. Electron. Mater. **37**, 815 (2008)
5. J.W. Yoon, H.S. Chun, S.B. Jung, J. Alloys Compd. **469**, 108 (2009)
6. R.W. Chuang, D. Kim, J. Park, C.C. Lee, IEEE Trans. Components Packag Technol. **27**, 177 (2004)
7. J.C. McNulty, Proc. – 2008 Int. Symp. Microelectron. IMAPS 2008 909 (2008)
8. S. Anhock, H. Oppermann, C. Kallmayer, R. Aschenbrenner, L. Thomas, H. Reichl, Proc. IEEE/CPMT Int. Electron. Manuf. Technol. Symp. 156 (1998)
9. O. Wada, T. Kumai, Appl. Phys. Lett. **58**, 908 (1991)
10. S.C. Yang, W.C. Chang, Y.W. Wang, C.R. Kao, J. Electron. Mater. **38**, 25 (2009)
11. J.H. Park, J.H. Lee, Y.H. Lee, Y.S. Kim, J. Electron. Mater. **31**, 1175 (2002)
12. H. Dong, V. Vuorinen, M. Broas, M. Paulasto-Kröckel, J. Alloys Compd. **688**, 388 (2016)

13. S.S. Kim, J.H. Kim, S.W. Booh, T.G. Kim, H.M. Lee, Mater. Trans. **46**, 2400 (2005)
14. J.Y. Tsai, C.W. Chang, C.E. Ho, Y.L. Lin, C.R. Kao, J. Electron. Mater. **35**, 65 (2006)
15. H.Q. Dong, V. Vuorinen, X.W. Liu, T. Laurila, J. Li, M. Paulasto-Kröckel, J. Electron. Mater. **45**, 566 (2016)
16. H.G. Song, J.P. Ahn, J.W. Morris, J. Electron. Mater. **30**, 1083 (2001)
17. H.Q. Dong, V. Vuorinen, T. Laurila, M. Paulasto-Kröckel, Calphad Comput. Coupling Phase Diagrams Thermochem **43**, 61 (2013)
18. J. Peng, R.C. Wang, H.S. Liu, J.Y. Li, J. Mater. Sci. Mater. Electron. **29**, 313 (2018)
19. P. Lin, W. Liu, Y. Ma, Y. Huang, S. Tang, J. Mater. Sci. Mater. Electron. **31**, 19013 (2020)
20. J.-M. Han, I.-J. Seo, Y. Ahn, Y.-S. Ko, T.-H. Kim, J. Korean Soc. Manuf. Technol. Eng. **23**, 355 (2014)
21. T. Tak-seng, D. Sun, H. Koay, M. Sabudin, J. Thompson, P. Martin, P. Rajkomar, S. Haque, EMAP2005. 118 (2005)
22. H.P. Park, G. Seo, S. Kim, K. one Ahn, Y.H. Kim (2019) J. Mater. Sci. Mater. Electron. **30**, 1055
23. H. Ru, V. Wei, T. Jiang, M. Chiu, Proc. Int. Microsystems, Packag. Assem. Circuits Technol. Conf. IMPACT 311 (2011)
24. J.W. Ronnie Teo, F.L. Ng, L.S. Kip Goi, Y.F. Sun, Z.F. Wang, X.Q. Shi, J. Wei, G.Y. Li, Microelectron. Eng. **85**, 512 (2008)
25. L.L. Liao, K.N. Chiang, J. Mech. **35**, 81 (2019)
26. S.W. Yoon, W.K. Choi, H.M. Lee, Acta Metall. **40**, 297 (1999)
27. A. Rautiainen, V. Vuorinen, H. Heikkinen, M. Paulasto-Krockel, IEEE Trans. Components Packag Manuf. Technol. **8**, 169 (2018)
28. I. Corporation, https://www.indium.com/technical-documents/product-data-sheets/download/3714 *(2017)*